von Willebrand factor conformation and adhesive function is modulated by an internalized water molecule

Reha Celikel[1], Zaverio M. Ruggeri[1,2] and Kottayil I. Varughese[1,2]

[1]Roon Research Center for Arteriosclerosis and Thrombosis, Division of Experimental Hemostasis and Thrombosis, Department of Molecular and Experimental Medicine and Department of Vascular Biology, The Scripps Research Institute, La Jolla, California 92037, USA. [2]Joint senior authors.

Platelet participation in hemostasis and arterial thrombosis requires the binding of glycoprotein (GP) Ibα to von Willebrand factor (vWF). Hemodynamic forces enhance this interaction, an effect mimicked by the substitution I546V in the vWF A1 domain. A water molecule becomes internalized near the deleted Ile methyl group. The change in hydrophobicity of the local environment causes positional changes propagated over a distance of 27 Å. As a consequence, a major reorientation of a peptide plane occurs in a surface loop involved in GP Ibα binding. This distinct vWF conformation shows increased platelet adhesion and provides a structural model for the initial regulation of thrombus formation.

Binding of the platelet membrane glycoprotein (GP) Ibα to von Willebrand Factor (vWF) immobilized on the vessel wall[1] initiates thrombus formation[2–4]. This process, essential to arrest bleeding at wound sites[5], may also contribute to thrombotic diseases such as myocardial infarction[6,7], and is modulated by the affinity of vWF for platelets. At the high wall shear rates typical of the arterial circulation, platelet adhesion to extracellular matrix components and thrombus growth depend on GP Ibα binding to the vWF A1 domain[3,4]. Platelets tethered to vWF roll with a velocity that, relative to freely moving cells, decreases progressively with increasing blood flow[2]. Thus, a greater shear stress may induce tighter GP Ibα binding to vWF and accelerate thrombus formation. Such a concept implies that either the A1 domain or GP Ibα, or both, can undergo conformational transitions that enhance their adhesive properties. Functional data support this hypothesis[8,9], but without direct structural evidence. Gain-of-function mutations in the vWF A1 domain[10] occur in patients with type 2B von Willebrand disease[11,12]. These mutant molecules, which express heightened binding to GP Ibα even in the absence of flow[13], may reveal conformations that exist in normal vWF only transiently during the process of adhesion, either as a consequence of immobilization onto specific substrates, the effect of shear forces, or both. To obtain information relating specific functional properties with distinct conformations of the A1 domain, we have crystallized the I546V gain-of-function mutant and solved its structure at 2.0 Å resolution. Our findings identify conformational transitions that may influence the vWF–GP Ibα interaction and modulate the initiation of platelet thrombus formation.

The vWF A1 domain has an α/β fold, with a β-sheet composed of six β-strands flanked by three α-helices on each side[14,15]. In the orientation shown in Fig. 1*a*, residue 546 in the α1-β2 loop is near the bottom of the molecule, below the β3-α2 loop. The I546V mutant and wild type A1 domain have similar overall structures, but the mutant can form tighter bonds with GP Ibα and tether platelets with remarkably lower rolling velocity than the wild type (Fig. 1*b*). We propose that the enhanced adhesive function of the mutant molecule is associated with structural changes that occur in the β2-β3 loop at a distance of 27 Å from residue 546 (Fig. 2). As a consequence of the I546V substitution, a water molecule (W1) enters the cavity left by the deleted Ile methyl group and forms a hydrogen bond with the carbonyl of Pro 574, shifting the residue by 0.42 Å and its torsion angle ψ by 15° (Fig. 2*a*). Consequently, small positional shifts occur in the β3-α2 loop, reflected by a movement of 0.44 Å in the Cα of Lys 572. These local changes are unlikely to have functional significance, but distant effects appear to be relevant. The Cε of Met 541, forced into a new orientation by the decreased hydrophobicity in the environment of W1, establishes a short contact with Cγ of Val 555. The latter residue shifts upward, but its side chain is packed within a hydrophobic environment and cannot assume a different rotomer position to relieve the strain. Propagation of the positional shift creates the space for a new water molecule (W2), which forms hydrogen bonds with one of the side chain carboxylate oxygens of Glu 557 and the hydroxyl of Tyr 565. The other carboxylate oxygen of Glu 557 forms a strong hydrogen bond with Nδ1 of His 559, pulling on the latter

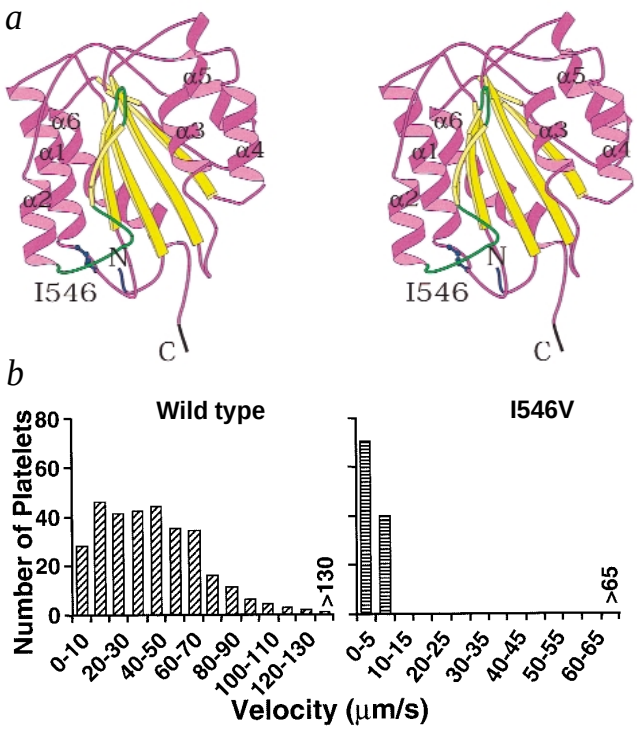

Fig. 1 Location of the I546V mutation and its effects on platelet adhesion. ***a***, Stereo view of the vWF A1 domain presented as a ribbon structure, with β-strands in yellow and α-helices in purple connected by loops. Note the position of the side chain of Ile 546. The loops preceding and following strand β3, site of the major conformational changes caused by the I546V substitution, are colored in green. The figure was produced with Bobscript[28]. ***b***, Velocity of platelets rolling on wild-type or I546V mutant vWF A1 domain in a flow field with wall shear rate of 1500 s^{-1}. Results are presented as number of platelets within defined velocity categories. Platelets rolling on the mutant A1 domain had a median velocity of 4.2 μm s^{-1} compared to 44.7 μm s^{-1} on the wild type control. A video clip showing the real time interaction of flowing platelets with wild type and mutant A1 domain is provided as supplementary material.

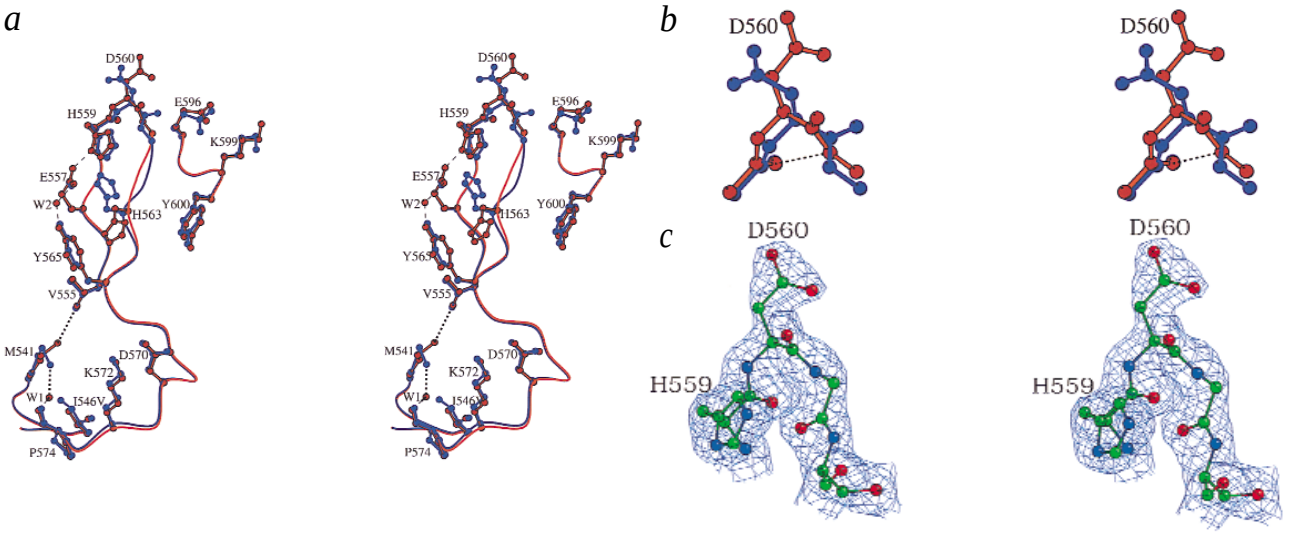

Fig. 2 Structural changes in the mutant A1 domain. ***a***, Partial stereo representation of wild type vWF A1 domain (blue) and I546V mutant (red). Cα atom traces and relevant side chains are shown in the segments of sequence 541–546 (part of helix α1 and loop α1-β2); 555–574 (part of strand β2, loop β2-β3, strand β3 and loop β3-α2); and 596–600 (part of helix α3). Repulsive forces are shown by thick dotted lines; new hydrogen bonds by thin dashed lines. ***b***, Stereo representation of the peptide sequence His 559, Asp 560 and Gly 561 (loop β2-β3) in the wild type (blue) and I546V mutant A1 domain (red). Carbon, oxygen and nitrogen atoms are shown as balls connected by sticks. The hydrogen bond between the carbonyl oxygen of His 559 and the amide of Gly 561, present only in the mutant molecule, is shown by a dotted line. ***c***, Stereo view of a σA weighted $2F_o - F_c$ map after refinement at 2.0 Å resolution showing the electron density of the residues from His 559 to Ser 562. Figure produced using Bobscript[28].

residue, and a drastic change occurs in the orientation of the Asp 560-Gly 561 peptide plane; originally parallel, it becomes perpendicular to the surface, causing the carbonyl of Asp 560 to point upward, and the amide of Gly 561 to point towards the inner core of the molecule (Fig. 2). The ψ angle of Asp 560 and the ϕ angle of Gly 561 change by 107° and -108°, respectively, and a new hydrogen bond between the carbonyl oxygen of His 559 and the amide of Gly 561, not present in the wild type structure (Fig. 2*b*), increases the stability of the sharp γ-turn in the loop connecting the antiparallel strands β2 and β3. Additionally, there are changes in the shape of the surface adjacent to this turn, as Cα of Ser 562 moves by 1 Å to the left and the side chain of His 563 is reoriented (Figs 2*a*, 3), as well as positional shifts in the main chain atoms that are propagated as far as the Cα of Ala 564. The Cα atoms of residues 560, 561, 562 and 563 move by 0.55, 0.66, 1.0 and 0.54 Å, respectively, and the side chains of residues 560 and 563 assume different rotomer positions.

The distant conformational effects of the I546V substitution alter the charge distribution of the exposed surface around the β2-β3 loop (Fig. 3). Asp 560 in the mutant displays a fully exposed carbonyl and a repositioned carboxylate that points towards the surface groove proposed to be involved in GP Ibα binding. Concurrently, because of the new position of the side chain of His 563, the carbonyl oxygen of Asp 520 and the side chain oxygen of Ser 562 become more exposed. Thus, the enhanced function of the I546V mutant may be explained by a new conformation, stabilized by the His 559–Gly 561 hydrogen bond, with a greater surface exposure of electronegative atoms that support stronger electrostatic interactions with GP Ibα. The observation that platelet

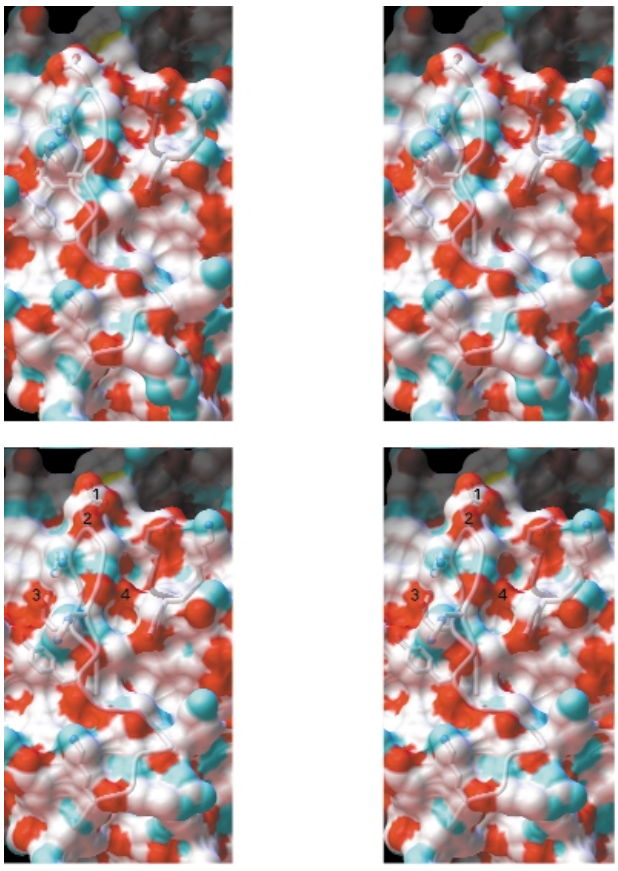

Fig. 3 Stereo representation of a partial surface of the vWF A1 domain wild type and I546V mutant. ***a***, Wild type; ***b***, I546V mutant. The tracing of Cα atoms and selected side chains are shown in the background. Electronegative oxygen atoms are colored in red; nitrogen atoms in blue. The view includes part of helix α1, loop α1-β2, strand β2, loop β2-β3, strand β3, loop β3-α2, and part of helix α3 (see Fig. 2*a*). Loop β2-β3 and helix α3 form the left and right hand sides, respectively, of a groove that may participate in binding platelet GP Ibα. Electronegative charge is increased in four locations of the mutant surface, labeled 1–4 in (*b*): 1, side chain of Asp 560; 2, carbonyl of Asp 560; 3, carbonyl of Asp 520; 4, side chain oxygen of Ser 562. This figure was produced using the program Reduced Surface[29].

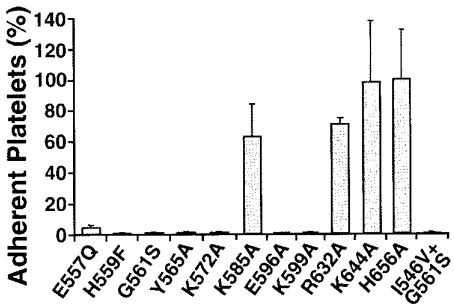

Fig. 4 Platelet adhesion to mutant vWF A1 domain fragments. Amino acid substitutions are indicated with the one letter code of the native and mutant residues. Single substitutions with Ala caused essentially complete loss of function at the following positions: Glu 557 in strand β2; His 559 in loop β2-β3; Tyr 565 in strand β3; Lys 572 in loop β3-α2; Glu 596 and Lys 599 in helix α3. The G561S substitution in the β2-β3 loop impaired the function of the wild type A1 domain as well as of the I546V mutant. In contrast, control mutations of Lys 585 in loop α2-α3, Arg 632 in helix α4, Lys 644 in loop α4-β5, and His 656 in loop β5-α5 had minimal or no effect on function. The number of surface interacting platelets was counted between 1 and 4 min from the beginning of flow; the wall shear rate was 1,500 s^{-1}. The results of mutant fragments are expressed as a percentage of those obtained with a wild type control tested on the same experimental day. The average number of platelets interacting with wild type vWF fragment was 57 (n = 11). The results represent the mean with standard error of the mean of two to four separate experiments performed with each mutant fragment.
Video clips can be viewed on the following web sites: *www.scripps.edu/mem/biochem/KI* and *www.scripps.edu/mem/eht/ruggeri.* These clips show the rolling of platelets, seen as white round objects, tethered to immobilized wild type A1 domain (top half of the screen) or I546V mutant A1 domain (lower half of the screen). The wall shear rate was 1500 s^{-1}. Platelets interacting with the mutant A1 domain roll with considerably lower velocity (median = 4.2 μm s^{-1}) than those interacting with the wild type control (median = 44.7 μm s^{-1}). The few larger objects that appear transiently in both screens and move rapidly are leukocytes that interact briefly with activated platelets on the surface.

adhesion to the A1 domain depends on the side chains of Asp 560 (ref. 16) and of the spatially proximal Glu 596 (Fig. 4) is in agreement with the conclusion that negative charge on the vWF surface is relevant for function. Of note, the best crystals of the mutant A1 domain were obtained when the molecule formed a complex with the antibody NMC-4. There are two published structures of the wild type A1 domain, one in complex with NMC-4 (ref. 14) and the other one uncomplexed[15], and they are essentially identical. Thus, it seems unlikely that binding of the antibody had any significant influence on the conformation described here.

Stable protein complexes are characterized by interacting surfaces complementary for shape and charge distribution. The binding of GP Ibα to the vWF A1 domain must be strong to oppose high shear stress while tethering platelets to surfaces, but is observed to be short lived[2,3]. These attributes indicate that the ligand and/or the receptor may possess structural flexibility that results in conformational isomerism, such that one conformation favors close association while another promotes fast dissociation. Conversely, in the I546V mutant, stabilization of the β2-β3 loop through a hydrogen bond, repositioning of the Asp 560-Gly 561 peptide plane, and rearrangement of negative charge around the strand β3-helix α3 groove (Figs 2*a*, 3) result in tighter GP Ibα binding (Fig. 1*a*). Interestingly, the G561S substitution[17] prevents even a molecule with the I546V mutation to support platelet tethering (Fig. 4), possibly because the side chain of the Ser residue precludes fitting of the receptor onto the proposed A1 domain binding surface[14]. This observation is consistent with the concept that positional changes in the adjacent β2-β3 loop mediate the functional effects of the I546V substitution. The β2-β3 loop, therefore, appears to have a key role in modulating initiation and stability of platelet adhesion to vWF. High crystallographic B-factors indicate that the β3-α2 loop (Fig. 1*a*), with one acidic and four basic residues in the sequence Lys 569-Asp-Arg-Lys-Arg 573 (ref. 14), is also flexible. Thus, isomeric conformations may exist in which either the Lys and Arg residues are poised for interaction with negatively charged GP Ibα residues, or the negatively charged Asp 570 is positioned for a repulsive kick off from the receptor. In agreement with this hypothesis, the side chain of Lys 572 is essential for support of platelet adhesion (Fig. 4).

The structural and functional characteristics of the I546V mutant indicate that distant areas of the globular A1 domain surface may participate in modulating GP Ibα binding, with an extended contact interface between ligand and receptor. We have verified this assumption by measuring platelet adhesion to immobilized vWF A1 domain in a flow field with high shear rate. We found that the residues required for normal function (Fig. 4) essentially correspond to those involved in the structural changes caused by the I546V gain-of-function substitution (Fig. 2*a*). These residues define an area of the A1 domain >20 Å in length, extending from the β2-β3 loop to the β3-α2 loop. It is presently unknown whether pathophysiological conditions exist that induce in normal vWF effects similar to the I546V mutation. At the onset of a response to vascular lesion, the binding of vWF to matrix components[3] and/or hemodynamic forces may induce positional shifts near residue 546, leading to the insertion of a water molecule into the A1 domain structure with the consequences shown here. Of note, these possibly reversible changes would only occur when vWF becomes part of insoluble supramolecular complexes and the interactions with GP Ibα are subjected to shear stress.

There is limited documentation on mutations resulting in the insertion of water molecules into a protein structure with perturbation of the protein conformation. The observed structural consequences are generally minor and localized, as seen for the substitution of Val 149 in T4 lysozyme with Ala[18] or Thr[19]. Only more drastic mutations, such as the insertion of one or more residues, typically cause wide ranging conformational transitions[20]. In the structure of triosephosphate isomerase, mutations in the active site cause changes in the ordered water molecules that affect the catalytic mechanism of the enzyme[21,22]. We now demonstrate that an internalized water molecule mediates the major distant effects of the conservative Ile to Val substitution in the vWF A1 domain structure, influencing a relevant event for thrombus formation under conditions compatible with the arterial circulation. Our results, therefore, illustrate a possible mechanism for the regulation of macromolecular interactions through solvent molecules.

Methods

Crystallization and structure solution. The method of expressing a vWF fragment with sequence 508–704 and the substitution I546V has been reported[23,24]. The complex of this mutant with the NMC-4 Fab was concentrated to ~10 mg ml^{-1} in 10 mM ammonium acetate, pH 7.5, and 60 mM calcium acetate[14]. Crystals were grown by vapor diffusion initially using the same conditions previously described for the wild type vWF A1 domain[14]. These conditions were then optimized using a reservoir solution with 12% (w/v) monomethyl ether polyethylene glycol 5000 in 0.12 M Tris-HCl, pH 7.3. The crystals belonged to the same C2 space group as reported for the wild type vWF A1 domain[14], and both mutant and wild

Table 1 Data collection and refinement statistics

Data collection	
Space group	C2
Cell constants[1]	a = 209.4 (208.2) Å
	b = 62.7 (61.9) Å
	c = 73.8 (72.9) Å
	β = 108.9° (108.6°)
Maximum resolution (Å)	2.0
Measured reflections	175,343
Unique reflections	57,228
Completeness (%)	93.2 (82.4)
R_{sym}[2] (%)	7.6 (40.8)
I / σ[2]	13.0 (2.3)
Refinement	
Resolution range (Å)	50.0–2.0
Reflections ($F > 2\sigma$)	47,739
R_{cryst} (%)	17.2
Number of reflections used in R_{free}	1,441
R_{free} (%)	20.7
Number of nonhydrogen protein atoms	4,901
Number of water molecules	636
R.m.s. deviations from ideal	
Bond lengths (Å)	0.005
Bond angles (°)	1.3
Ramachandran plot	
Most favored (%)	90.7
Additional allowed (%)	8.8

[1]Values in parentheses correspond to the wild type A1 domain–NMC4 complex.
[2]Values in parentheses correspond to the highest shell (2.07–2.0 Å).

type crystals had almost identical cell constants. Diffraction data at 2.0 Å resolution were collected at the beam line 7-1 in the Stanford Synchrotron Radiation Laboratory using a MAR image plate. A total of 184 images were collected at 90 K after flash freezing the crystal, with a $\Delta\Phi$ of 1°. Statistics of data collection and refinement are provided in Table 1. The structure of the I546V mutant was solved using the wild type A1 domain–NMC-4 Fab complex as a starting model[14]. Rigid body refinements were performed with X-PLOR[25] in two steps, at 15–6 Å and 15–2.5 Å. In each step, refinements were carried out at three levels: treating the whole complex as one rigid body; treating the A1 domain and NMC-4 Fab as two groups; treating the variable and constant domains of the light and heavy chains of the NMC-4 Fab as separate groups, and the A1 domain as the fifth group. The R-factor at this point was 34.9%. $F_o - F_c$ and $3F_o - 2F_c$ electron density maps were computed, and necessary corrections were made in the model. Slow cool, positional, B-group, and restrained individual B refinements decreased the R-factor to 24.7% and R_{free} to 31%. Omit maps were computed leaving out 50 residues of the mutant A1 domain that appeared to have undergone positional changes compared to the wild type. The model was rebuilt and refined with the maximum likelihood procedure and bulk solvent correction, using the program CNS[26], yielding a final R-factor of 17.2% and R_{free} of 20.7%.

Platelet adhesion to the vWF A1 domain in a flow field. Recombinant polypeptides comprising residues 445–733 of the mature vWF subunit, either with wild type sequence or specific amino acid substitutions, were expressed as described[23]. The fragments were immobilized onto glass cover slips at a coating concentration of 100 μg ml^{-1}, sufficient to saturate the surface[8]. Perfusion studies were performed with blood cells removed from plasma and resuspended in an equivalent volume of modified HEPES-Tyrode buffer, pH 7.4, containing 50 mg ml^{-1} of bovine serum albumin and 5 mM EDTA[8]. The platelet count in the cell suspension was lowered to between 9,000 and 12,000 per μl in order to decrease interacting platelets on the surface and facilitate image analysis. Interactions between surface bound vWF A1 domain and platelet GP Ibα in flowing blood were observed in real time by epifluorescence videomicroscopy[2,8]. Blood cells were labeled with 10 μm quinacrine hydrochloride (mepacrine) and aspirated through a parallel plate chamber, at 37 ºC, with flow rate of 0.484 ml min^{-1}, producing a wall shear rate of 1,500 s^{-1} at the inlet[2,27]. Individual platelets interacting with immobilized vWF fragments were counted on single frames from real time (30 frames per second) recordings. Analysis was performed on stacks of 10 digitized images captured randomly at 2–5 s intervals between 1 and 4 min from the onset of blood flow. Background fluorescence, defined as the average of several images of the surface without adherent platelets in focus, was subtracted from all processed images. After adjusting brightness and contrast, a threshold was applied to distinguish platelets from noise and images were binarized. Adherent platelets were counted on an area of 25,600 μm^2. The velocity of platelets rolling onto the vWF A1 domain coated surface was measured as described[2].

Coordinates. Coordinates of the structure described here have been deposited with the Protein Data Bank (accession code 1FNS).

Acknowledgments
We thank J. Ware for his assistance in the preparation of recombinant proteins and valuable suggestions during this entire project. We are also indebted to J.R. Roberts and R.A. McClintock for the expression and purification of vWF fragments and NMC-4 Fab; to J.A. Dent for assistance with the flow studies; to R. Habermann for help with image analysis and video editing; to U. Sen for assistance in computation; to M. Pique for preparing Fig. 4; and to B. Mathews for discussing the lysozyme mutants. This work was supported by National Institutes of Health grants and by the Rose and Sam Stein fund. The X-ray diffraction facilities were provided by N.H. Xuong at University of California, San Diego and the Stanford Synchrotron Radiation Laboratory.

Correspondence should be addressed to K.I.V. *email: kiv@scripps.edu* or Z.M.R. *email: ruggeri@scripps.edu*

Received 30 March, 2000; accepted 25 July, 2000.

1. Ruggeri, Z.M. In *von Willebrand factor and the mechanisms of platelet function*. (ed., Ruggeri, Z.M.), 33–77 (Springer, Berlin; 1998).
2. Savage, B., Saldivar, E. & Ruggeri, Z.M. *Cell* **84**, 289–297 (1996).
3. Savage, B., Almus-Jacobs, F. & Ruggeri, Z.M. *Cell* **94**, 657–666 (1998).
4. Ruggeri, Z.M., Dent, J.A. & Saldivar, E. *Blood* **94**, 172–178 (1999).
5. Tschopp, T.B., Weiss, H.J. & Baumgartner, H.R. *J. Lab. Clin. Med.* **83**, 296–300 (1974).
6. Fuster, V., Badimon, L., Badimon, J.J. & Chesebro, J.H. *N. Engl. J. Med.* **326**, 242–250 (1992).
7. Fuster, V., Badimon, L., Badimon, J.J. & Chesebro, J.H. *N. Engl. J. Med.* **326**, 310–318 (1992).
8. Miyata, S. & Ruggeri, Z.M. *J. Biol. Chem.* **274**, 6586–6593 (1999).
9. Marchese, P., Saldivar, E., Ware, J. & Ruggeri, Z.M. *Proc. Natl. Acad. Sci. USA* **96**, 7837–7842 (1999).
10. Ware, J. *et al. Proc. Natl. Acad. Sci. USA* **88**, 2946–2950 (1991).
11. Ruggeri, Z.M., Pareti, F.I., Mannucci, P.M., Ciavarella, N. & Zimmerman, T.S. *N. Engl. J. Med.* **302**, 1047–1051 (1980).
12. Ruggeri, Z.M. & Zimmerman, T.S. *J. Clin. Invest.* **65**, 1318–1325 (1980).
13. De Marco, L., Girolami, A., Zimmerman, T.S. & Ruggeri, Z.M. *Proc. Natl. Acad. Sci. USA* **82**, 7424–7428 (1985).
14. Celikel,R., *et al. Nature Struct. Biol.* **5**, 189–194 (1998).
15. Emsley, J., Cruz, M., Handin, R. & Liddington, R. *J. Biol. Chem.* **273**, 10396–10401 (1998).
16. Cruz, M.A. *et al. J. Biol. Chem.* **275**, 19098–19105 (2000).
17. Rabinowitz, I., *et al. Proc. Natl. Acad. Sci. USA* **89**, 9846–9849 (1992).
18. Xu, J., Baase, W.A., Baldwin, E. & Matthews, B.W. *Protein Sci.* **7**, 158–177 (1998).
19. Blaber, M. *et al. Biochemistry* **32**, 11363–11373 (1993).
20. Vetter, I.R., *et al. Protein Sci.* **5**, 2399–2415 (1996).
21. Komives, E.A., *et al. Biochemistry* **34**, 13612–13621 (1995).
22. Zhang, Z., *et al. Biochemistry* **38**, 4389–4397 (1999).
23. Miyata, S., Goto, S., Federici, A.B., Ware, J. & Ruggeri, Z.M. *J. Biol. Chem.* **271**, 9046–9053 (1996).
24. Federici, A.B., *et al. Thromb. Haemost.* **78**, 1132–1137 (1997).
25. Brünger, A.T. *X-PLOR crystallographic program suite (Version 3.851).* (Yale University Press, New Haven, Connecticut; 1996).
26. Brünger, A.T., *et al. Acta Crystallogr. D* **54**, 905–921 (1998).
27. Usami, S., Chen, H.H., Zhao, Y., Chien, S. & Skalak, R. *Ann. Biomed. Eng.* **21**, 77–83 (1993).
28. Esnouf, R.M. *J. Mol. Graph Model* **15**, 132–134 (1997).
29. Sanner,M.F., Olson,A.J. & Spehner,J.C. *Biopolymers* **38**, 305–320 (1996).